

Geophysical Research Letters

RESEARCH LETTER

10.1002/2016GL070175

Key Points:

- Moment tensors show that principal stress directions at the New Madrid seismic zone are 30° different than surrounding regions
- Faults at New Madrid incompatible with regional stress but optimally aligned in local stress field
- Stress due to dense lower crust and tectonic stress interfere constructively, causing a regional deviatoric stress maximum at New Madrid

Supporting Information:

- Supporting Information S1

Correspondence to:

W. Levandowski,
wlevandowski@usgs.gov

Citation:

Levandowski, W., O. S. Boyd, and L. Ramirez-Guzmán (2016), Dense lower crust elevates long-term earthquake rates in the New Madrid seismic zone, *Geophys. Res. Lett.*, 43, doi:10.1002/2016GL070175.

Received 18 FEB 2016

Accepted 26 JUL 2016

Dense lower crust elevates long-term earthquake rates in the New Madrid seismic zone

Will Levandowski¹, Oliver S. Boyd¹, and Leonardo Ramirez-Guzmán²

¹U.S. Geological Survey Geologic Hazards Science Center, Golden, Colorado, USA, ²UNAM, Mexico City, Mexico

Abstract Knowledge of the local state of stress is critical in appraising intraplate seismic hazard. Inverting earthquake moment tensors, we demonstrate that principal stress directions in the New Madrid seismic zone (NMSZ) differ significantly from those in the surrounding region. Faults in the NMSZ that are incompatible with slip in the regional stress field are favorably oriented relative to local stress. We jointly analyze seismic velocity, gravity, and topography to develop a 3-D crustal and upper mantle density model, revealing uniquely dense lower crust beneath the NMSZ. Finite element simulations then estimate the stress tensor due to gravitational body forces, which sums with regional stress. The anomalous lower crust both elevates gravity-derived stress at seismogenic depths in the NMSZ and rotates it to interfere more constructively with far-field stress, producing a regionally maximal deviatoric stress coincident with the highest concentration of modern seismicity. Moreover, predicted principal stress directions mirror variations (observed independently in moment tensors) at the NMSZ and across the region.

1. Introduction

The New Madrid seismic zone (NMSZ) hosts the highest concentration of natural seismicity in the Central and Eastern United States (CEUS; Figure 1a) and produced the region's three largest historical earthquakes, the magnitude 7–8 events of 1811–1812 [Johnston, 1996; Hough and Page, 2011; Boyd and Cramer, 2014; Cramer and Boyd, 2014]. Paleoseismic studies suggest similar large earthquake sequences around 1450, 900 A.D., and older [Tuttle et al., 2002, 2005]. Nevertheless, geodetic strain rates are $10^{-9}/\text{yr}$ or less, near or below the threshold detectable [Craig and Calais, 2014; Boyd et al., 2015], and Holocene rates of seismicity are 1–2 orders of magnitude greater than on average through the Cenozoic [e.g., Schweig and Ellis, 1994], consistent with the episodic activity observed on intraplate faults worldwide [e.g., Clark et al., 2012]. Therefore, determining whether long-term stress is elevated in the NMSZ or whether such large but episodic seismicity is expected elsewhere/everywhere in the CEUS is of paramount importance to assessing seismic hazard.

Modern NMSZ earthquakes are dominantly right lateral on the steeply dipping, ENE striking Cottonwood Grove fault (CWG) and a more diffuse, ENE trending set of faults in the northern Mississippi Embayment (NME; Figure 1d) and reverse on the SSE striking Reelfoot Thrust [Johnson et al., 2014; Shumway, 2008]. Earthquake moment tensors reflect ~E-W maximal compression (σ_1) with the N-S and vertical principal components roughly equal in magnitude. This orientation is nearly optimal to exploit SSE striking faults as thrusts and NNE strands as strike slip (i.e., anomalously weak faults are not required [Hurd and Zoback, 2012a]). Yet elsewhere in the CEUS, maximal horizontal compression (σ_{Hmax}) trends ENE-WSW, resulting from compression transmitted from Mid-Atlantic Ridge spreading (the North American-Eurasian plate boundary) [e.g., Zoback and Zoback, 1980; Richardson, 1992; Humphreys and Coblenz, 2007] and/or basal shear imparted by asthenospheric flow [e.g., Forte et al., 2007; Ghosh et al., 2013]. Additionally, strike slip predominates in the region surrounding the NMSZ (i.e., $\sigma_{\text{Hmax}} > \sigma_{\text{vertical}} > \sigma_{\text{Hmin}}$). Thus, the relative magnitudes of principal stress in the NMSZ ($\sigma_{\text{Hmax}} \approx \sigma_{\text{vertical}} > \sigma_{\text{Hmin}}$) differ from in its surroundings, and the orientations of the principal axes are rotated some 30° clockwise.

The net loading of intraplate faults is the tensor sum of the loads transmitted from the plate edges and base and those due to gravitational body forces. Topographic gradients and regions of anomalous crustal and/or upper mantle density create lateral disequilibria in lithostatic pressure that serve as a localized source of stress [e.g., McGarr, 1988], for example. And because tectonism may thicken or thin the crust, emplace igneous intrusions, cause metamorphism, or alter lithospheric density in any number of other ways, anomalous densities (in addition to faults) may be expected in zones of prior deformation.

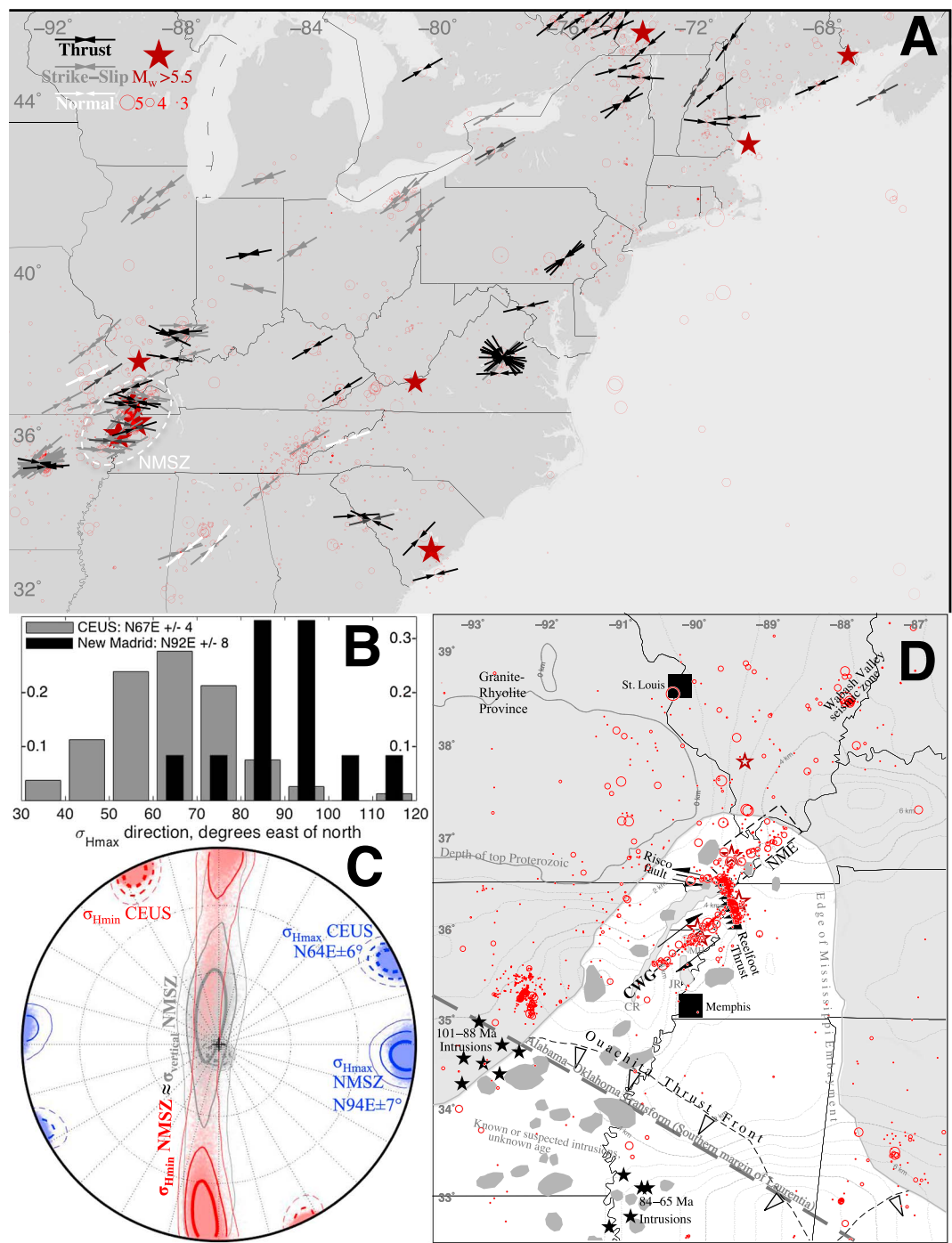


Figure 1. (a) Seismicity and σ_{Hmax} directions. Moment tensors reflect ENE-WSW σ_{Hmax} in the CEUS and ~E-W σ_{Hmax} in the NMSZ. Seismicity includes all events since 1974 (circles) [earthquake.usgs.gov/earthquakes/search/] and $M_w > 5.5$ prior (stars) [Petersen et al., 2014]. (b) Histograms of σ_{Hmax} trend inferred from individual moment tensors. (c) Principal stress axes from moment tensor inversion (upper hemisphere projection). The dashed/solid lines are the 1σ , 2σ , and 3σ confidence contours in CEUS/NMSZ. Blue denotes σ_1 , gray σ_2 , and red σ_3 . In the NMSZ, σ_1 is horizontal, $N94E \pm 7^\circ$ (2σ), and $\sigma_2 \approx \sigma_3 \approx \sigma_{vertical} \approx \sigma_{Hmin}$. In the CEUS, σ_1 is $N64E \pm 6^\circ$, $\sigma_2 \approx \sigma_{vertical}$, and σ_3 is horizontal. The two regions differ to 99.9% confidence. (d) Tectonic map of the NMSZ and surroundings. CWG: Cottonwood Grove fault, NME: NNE to NE trending faults and epicenter alignments of the northern Mississippi Embayment, CR: Crowley's Ridge, JR: Joiner Ridge, MH: Manila High.

Indeed, the Quaternary-ongoing rejuvenation of the NMSZ is part of a long history of episodic deformation in and near the Early Cambrian Reelfoot rift [Ervin and McGinnis, 1975]. Late Paleozoic (Ouachita) NW-SE contraction impinged on the southernmost end of the modern NMSZ (Figure 1d) [e.g., Hatcher et al., 1989], and left-lateral slip on preexisting NE striking faults may have occurred throughout the modern NMSZ [Langenheim and Hildenbrand, 1997; Csontos et al., 2008]. Numerous plutons of unknown age—but generally posited to be Middle/Late Cretaceous—are documented in seismic surveys or inferred from potential field data, and Cretaceous/Tertiary (thermal?) subsidence created accommodation space for the sedimentary fill of the Mississippi Embayment [Cox and Van Arsdale, 2002]. Dated, Late Cretaceous intrusions and Neogene-Quaternary normal faults [Hao et al., 2015] abound southwest of the NMSZ, likely manifestations of multiple reactivations of the Proterozoic southern margin of Laurentia [Cox et al., 2013]. Irregularly periodic but recurrent Cenozoic slip (generally dextral to reverse-oblique) has migrated among numerous subparallel faults in the Mississippi Embayment [Pratt, 1994; Johnston and Schweig, 1996; Cox et al., 2006].

Features inherited from this repeated tectonism have been previously suggested as the cause of modern seismicity in the NMSZ. Such hypotheses broadly fall into two categories: zones of weakness and gravitational body forces. Rheologically weak lower crust [Liu and Zoback, 1997; Kenner and Segall, 2000; Pollitz et al., 2001] and/or upper mantle [Grollimund and Zoback, 2001; Pollitz and Mooney, 2014, 2016] would strain accordingly faster in the regional stress field, and unless the brittle and ductile regimes become decoupled the whole lithosphere strains at essentially the same rate over geologic time. Stress in the brittle regime remains near the ~ 100 MPa yield stress, and the few megapascal of coseismic stress drop typical of intraplate earthquakes is reloaded [Liu and Zoback, 1997; Zoback and Townend, 2001] by the deformation of the underlying ductile material. As such, rheologic weakness is an appealing mechanism for the high seismicity rates in the NMSZ, but it does not explain the observed reorientation of σ_{Hmax} . By contrast, an additional, local source of stress with distinct σ_{Hmax} could cause a rotation of net principal stresses and an increase in loading stress, elevating seismicity rates.

Previous hypotheses invoking gravity-derived stress noted high-velocity, presumably dense lower crust imaged in refraction studies and inferred to be Cretaceous, mafic intrusions [Ginzburg et al., 1983; Mooney et al., 1983]. Idealizing this body as a rectangular anomaly of $+200 \text{ kg/m}^3$ at 25–32.5 km depth, Grana and Richardson [1996] modeled residual stress 100 m.y. after its emplacement (i.e., assuming intrusions are mid-Cretaceous in age). Their model estimates 30–150 MPa of body force-derived WNW-ESE compression in the seismogenic crust. Consequently, it requires 45–80 MPa ENE-WSW regional stress in order to reproduce σ_{Hmax} orientations. Pollitz et al. [2001] chose a $+150 \text{ kg/m}^3$ cylindrical anomaly (15 km radius). Imposing instantaneous weakening of the lower crust to a viscosity of $1.5 \times 10^{19} \text{ Pa s}$ (below the lower bound of 10^{21} Pa s in the NMSZ [Boyd et al., 2015]) allows the dense body to sink, stressing the overlying seismogenic crust by a much more modest 1–3 MPa.

These models that invoke idealized densities and ad hoc rheologies demonstrate that gravity-derived stress could focus seismicity. At present, however, we seek to aid in the assessment of seismic hazard in the populous St. Louis-Memphis region by mapping elevations and suppressions of long-term fault loading. As such, we require a realistic 3-D density structure, which we derive by joint analysis of a regional crustal velocity model [Ramirez-Guzmán et al., 2012], gravity, and topography. This density model then forms the input to 3-D finite element models of the present-day gravity-derived loading in the NMSZ and its interactions with far-field stress and known faults.

2. Principal Stress Directions in the CEUS

The trend of σ_{Hmax} in the NMSZ appears distinct from that in the rest of the CEUS (Figure 1b) [e.g., Grana and Richardson, 1996; Hurd and Zoback, 2012b]. We invert 88 moment tensors from the CEUS and 15 from the NMSZ [Hermann, 2015] for the optimal stress tensor in each region (with code modified from Vavryčuk [2014]). To assess uncertainty, we conduct 50,000 inversions. In each, perturbations of $\pm 15^\circ$ are added to the slip vectors, the input population is bootstrap-resampled, and a random coefficient of friction between 0.4 and 1.0 is chosen. The resultant σ_{Hmax} directions are $\text{N}64\text{E}\pm 6^\circ$ in the CEUS and $\text{N}94\text{E}\pm 7^\circ$ in the NMSZ (2σ); these populations differ to 99.9% confidence (Figures 1b and 1c).

This rotation has important consequences and implications. The ENE striking CWG and NME faults nearly parallel regional σ_{Hmax} . These faults would not be suitable for strike-slip motion. Yet the rotation of principal

stress at the NMSZ orients these planes well for failure ($\sim 25\text{--}35^\circ$ from local σ_1). Knowing only fault orientations, presuming that the state of stress is uniform across the CEUS could lead to an underappreciation of the risk of damaging shaking in the NMSZ. Thus, understanding the local stress field is crucial when considering the hazard associated with intraplate faults.

3. The 3-D Density Model

3.1. Methodology

Previously, dynamic models have shown that lateral density variations similar to those suspected in the NMSZ may locally elevate deviatoric stress. Because we are interested in modern seismic hazard and aim to produce a 3-D stress map for use in understanding the likely spatial distribution of future seismicity, we require a realistic rather than idealized lithospheric model as input to quasi-static finite element simulations of gravity-derived stress. The derivation of this model closely follows the approach of *Levandowski et al.* [2015] (to which readers are referred for details of the method), summarized briefly here.

Lithospheric density generally mirrors seismic velocity variations, but more importantly, it must reproduce gravity and flexural topography variations. *Ramirez-Guzmán et al.* [2012] assembled a high-resolution crustal velocity model, tested and calibrated with ground-motion simulations of the $M_w 5.4$ Mt. Carmel, Illinois, earthquake. Nevertheless, scaling this velocity model to density through an empirical regression (based on data from *Christensen* [1996] and *Brocher* [2005])

$$\rho = -15.84v_s^5 + 209.13v_s^4 + -961.94v_s^3 + 1863.36v_s^2 + -1163.00v_s + 2153.06 \quad (1)$$

does not perfectly recover gravity and topography. (To account for lithospheric flexure, we convolve the 1-D (Airy) buoyancy with the flexural Green's functions, a system of zero-order Kelvin-Bessel functions [*Watts*, 2001, equations (3.54) and (3.55)], and smooth the observed elevation with the same filter.) L1 norms of residual gravity and flexurally modulated topography are 26 mGal and 103 m, respectively. Notably, this velocity-density regression (equation (1)) systematically underestimates the density of mafic rocks and overestimates the density of felsic units, and moreover, the crustal model overlies homogeneous mantle.

In order to reconcile our model with gravity and topography, we refine this initial density estimate, implicitly allowing deviations from equation (1) in the crust and allowing density variations in the mantle to arise as needed to fit the data. We divide the region into a 10×10 km grid and interpolate observed free air gravity and topography [*Dater et al.*, 1999] onto this grid. The lithosphere is divided into nine layers: surface to sea level, 0–5, 5–15, 15–25, 25–35, 35–50, 50–85, 85–120, and 120–150 km below sea level. The initial density is derived from the velocities of *Ramirez-Guzmán et al.* through equation (1) (and is uniform in the mantle). We then conduct 1000 simulations as follows: each begins by randomly choosing a laterally uniform elastic thickness of 60 ± 20 km [*Kirby and Swain*, 2009; *Watts*, 2012] and then calculating the gravity and flexurally modulated topography predicted by the initial density model. These initial predictions are compared to observations, and then a random walk Monte Carlo algorithm iteratively refines the density model until residuals at all points in the study area are below 5 mGal and 50 m (typical L1 norms of < 2 mGal and < 20 m: variance reduction $\sim 99\%$). Results discussed below are the means across these 1000 simulations (2σ ranges thereof are universally < 2 kg/m³).

3.2. Results

The primary crustal structures in our model are previously known from geologic and/or geophysical constraints. The dichotomy between bedrock outside of the Mississippi Embayment and rift-fill sediments within it dominates at shallow depths (Figure 2a). This pattern reverses in the lower crust (Figure 2c): dense, mafic rocks in the rift contrast with the felsic granite-rhyolite province to the northwest. The lower crust is dense throughout the Mississippi Embayment, but the body beneath the NMSZ is unique, ~ 200 kg/m³ denser than its surroundings.

The starting model is uniform in the mantle, but density variations emerge with the inclusion of gravity and topography. Thinned and/or dense lower crust in the Mississippi Embayment underlies low-density sediments; our initial model roughly reproduces elevation there but underestimates gravity by up to 50 mGal (likely because equation (1) underestimates the density of mafic lithologies). As the model is refined, much

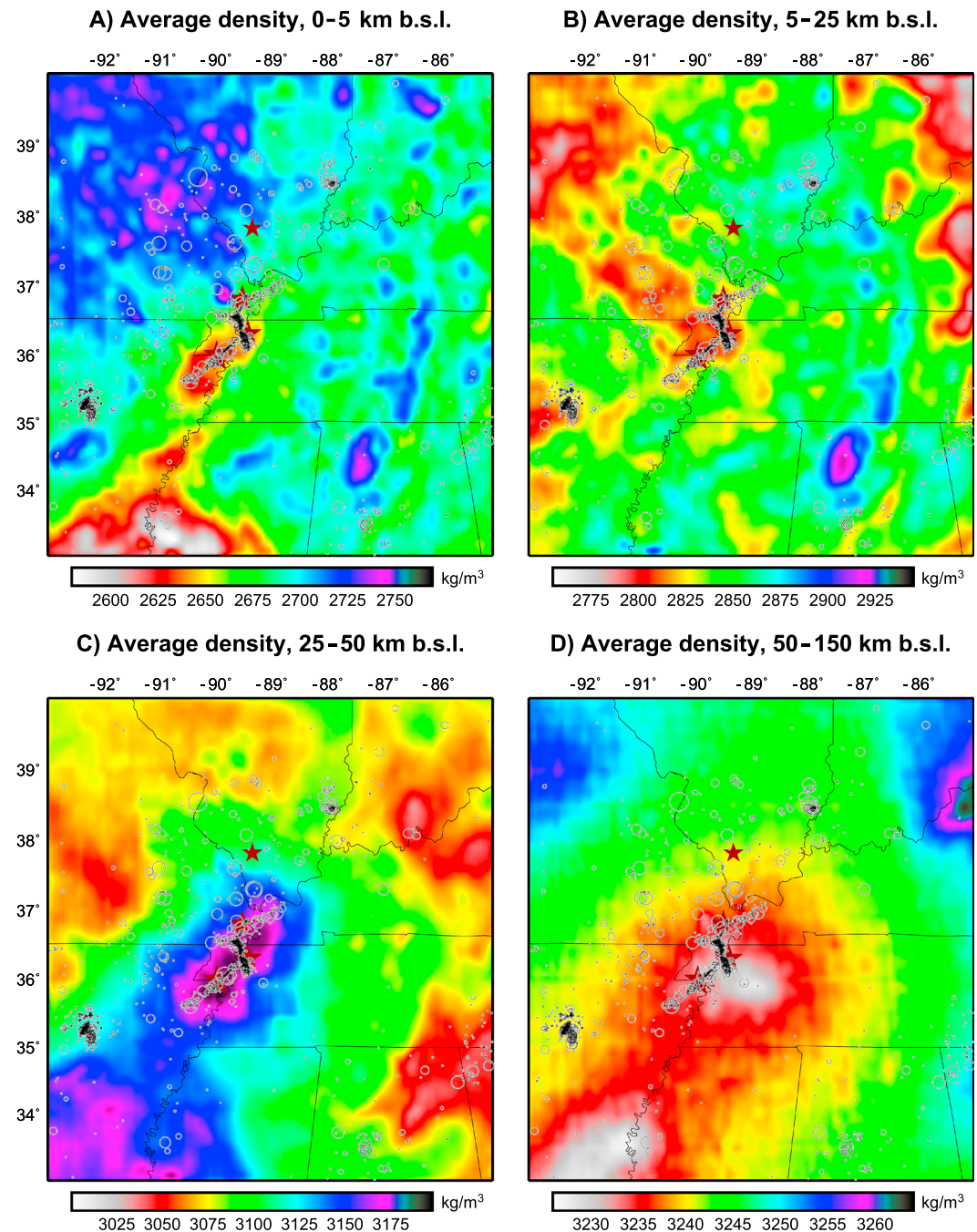


Figure 2. (a–d) Density model, the mean across 1000 simulations averaged over the depth ranges noted.

of the crust becomes $\sim 60 \text{ kg/m}^3$ denser but the mantle more buoyant. The final models suggest a $\pm 20 \text{ kg/m}^3$ density range across the region at 85–150 km depth (Figure 2d).

This pattern resembles tomographic images, with velocities $\sim 5\%$ lower beneath the Reelfoot rift than beneath the granite-rhyolite province [Pollitz and Mooney, 2014, 2016; Schmandt and Lin, 2014]. These velocity and density variations could reflect either thermal or compositional heterogeneity. Temperature variations of $\pm 150^\circ\text{C}$ accounts for both the $\pm 20 \text{ kg/m}^3$ density variations and $\pm 2\%$ range of S velocity [e.g., Levandowski *et al.*, 2015]. Unifying velocity and density with compositional variations is more difficult. Melt depletion during one of the multiple stages of magmatism would have decreased density but *increased* velocity [Lee, 2003; Schutt and Lesher, 2010]. Similarly, upper mantle hydration does lower both velocity

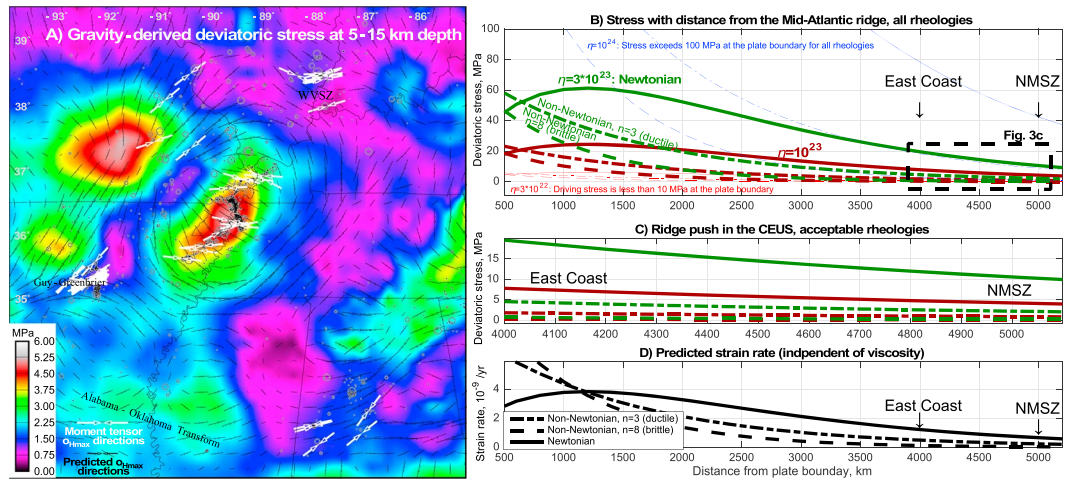


Figure 3. Gravity-derived and tectonic stresses. (a) The 3-D finite element model of gravity-derived stress (not considering far-field stress) at seismogenic depths. (b) Plate-boundary stress. The Mid-Atlantic Ridge is at 0 km. The thick lines are the acceptable models (i.e., stress at the ridge >10 MPa and <100 MPa); the thin lines are the unacceptable models. The solid lines denote Newtonian; dot-dashed lines non-Newtonian, $n=3$; and dashed lines non-Newtonian, $n=8$. The colors denote the bulk viscosity as labeled. (c) Regional stress in the CEUS is 0–20 MPa and <10 MPa (likely 0–5 MPa) in the NMSZ. (d) Strain rates normal to the plate boundary predicted from ridge push ($\sim 10^{-9}$ /yr) are similar to geodetic estimates [Calais et al., 2010; Frankel et al., 2012; Boyd et al., 2015].

and density, but the 40 kg/m^3 range in density would correspond to $<1\%$ velocity variation [Schutt and Lesher, 2010]. Therefore, we favor a thermal rather than compositional origin for this velocity/density pattern, such as thinner lithosphere beneath the Reelfoot rift than its surroundings.

4. Stress Modeling

The local, intraplate stress tensor is the sum of those due to body forces and far-field loading, here Mid-Atlantic Ridge push and/or basal shear. Therefore, it is essential to estimate both the stress perturbations due to density structure and the far-field stress upon which they are superimposed.

4.1. Plate-Boundary Loading

Arguments based on geoid anomalies [Turcotte and Schubert, 2002], torque balance [Richardson, 1992], and transform-valley bathymetry [Luttrell and Sandwell, 2012] all estimate 20–50 MPa of ridge push along the plate boundary, but the magnitude of deviatoric stress transmitted into the North American interior is unknown. We derive analytical solutions for deviatoric loading from the Mid-Atlantic Ridge (Figure 3b) by idealizing the North American lithosphere as a uniform viscous medium and approximating ridge push as a constant-velocity boundary condition. In Newtonian media under plane stress, the edge-normal velocity, V , as a function of distance, y , from a plate boundary of length scale $2L$ is [England et al., 1985]

$$V(y) = V_{y=0} e^{-\frac{2\pi y}{L}} \left(1 + \frac{2\pi y}{L} \right) \quad (2)$$

Strain rate, $\dot{\epsilon}_{yy}$, is the gradient of velocity

$$\dot{\epsilon}_{yy} = \frac{dV}{dy} = -4V_{y=0}\pi^2 y e^{-\frac{2\pi y}{L}} / L^2 \quad (3)$$

Finally, strain rate is proportional to viscosity (η) and deviatoric stress:

$$\sigma_{yy} = 2\dot{\epsilon}_{yy}\eta = -8\eta V_{y=0}\pi^2 y e^{-\frac{2\pi y}{L}} / L^2 \quad (4)$$

Equations (1)–(3) are subject to several constraints. The strain rate near New Madrid, ~ 5000 km from the plate boundary, is at most $\sim 10^{-9}/\text{yr}$, near or below the rate detectable with existing GPS data [Craig and Calais, 2014; Boyd et al., 2015]. Second, the velocity at the plate boundary is half of the 2.5 cm/yr spreading rate of

the Mid-Atlantic Ridge. Third, the stress near the plate boundary should be tens of megapascal, as independently estimated from the geoid, torque balance, and transform-valley bathymetry [Richardson, 1992; Turcotte and Schubert, 2002; Luttrell and Sandwell, 2012]. Finally, η must exceed 10^{21} Pa s in the NMSZ [Boyd et al., 2015]. (Vertically averaged viscosity in North America ranges from 10^{22} to 10^{24} Pas [Walcott, 1970].)

Reassuringly, the 5000–10,000 km length scale of the Mid-Atlantic Ridge (using equation (3)) predicts strain rates across the CEUS of $0.1\text{--}2 \times 10^{-9}/\text{yr}$ (Figure 3d). For this length scale and strain rate, viscosities greater than 3×10^{23} and less than 4×10^{22} Pa s require ridge push of greater than 100 MPa and less than 10 MPa, respectively (equation (4) and Figure 3b), inconsistent with independent estimates. This acceptable viscosity range predicts deviatoric loads of 1–10 MPa in the NMSZ (Figure 3c).

In non-Newtonian media, equations (1)–(3) become [England et al., 1985]

$$V(y) = V_{y=0} e^{-\frac{\sqrt{n}\pi y}{L}} \quad (5)$$

$$\dot{\epsilon}_{yy} = \frac{dV}{dy} = -V_{y=0} \sqrt{n\pi/L} e^{-\frac{\sqrt{n}\pi y}{L}} \quad (6)$$

$$\sigma_{yy} = B \dot{\epsilon}^{(\frac{1}{n}-1)} \dot{\epsilon}_{yy} \quad (7)$$

The constant n represents the proportion of brittle deformation (for pure ductile creep, $n=3$; higher n reflect greater contributions from brittle mechanisms). $\dot{\epsilon}$ is the second invariant of the local strain rate tensor. B is a constant that describes the vertically averaged temperature dependence of viscosity. For all parameter choices that satisfy the geodetic and physical constraints listed above, loading of the NMSZ by ridge push is 0.1–5 MPa (Figure 3c).

The mean loading predicted across acceptable models is 3.0 MPa, ranging from 0.1 MPa (non-Newtonian, $n=8$, $\eta=4 \times 10^{22}$ Pa s) to 10.0 MPa (Newtonian, $\eta=3 \times 10^{23}$ Pa s).

4.2. Basal Shear

If instead the regional stress field in eastern North America is dominated by basal shear from asthenospheric flow, the magnitude of deviatoric horizontal normal stress in the seismogenic crust is not estimated so easily, since it depends on the geometry and velocity of convective currents, the coupling between lithosphere and asthenosphere (a function of differential velocity and viscosity structure), and the degree to which material below seismogenic depths transmits basal shear loading upward. Many convection models estimate magnitudes of basal shear exceeding the 0.1–10 MPa that we estimate from ridge push [Becker and O'Connell, 2001; Forte et al., 2007; Ghosh et al., 2013]. Nevertheless, in attempting to solve for the magnitudes of edge stress along individual plate-boundary segments and basal shear (with spatial distribution and relative magnitudes defined by global convection models [Becker and O'Connell, 2001]) that, when summed with gravitational potential energy variations, best reproduces World Stress Map observations, Humphreys and Coblenz [2007] argue that the loads transferred to the seismogenic crust from basal shear are ~20% of the basal traction. As such, the ~20 MPa of ENE traction estimated beneath the NMSZ by Forte et al. [2007] plausibly results in similar long-wavelength loading (1 MPa) as we estimate from Mid-Atlantic ridge push.

This magnitude is similar to numerous estimates of intraplate deviatoric loading [Jones et al., 1996; Flesch et al., 2007; Humphreys and Coblenz, 2007; Ghosh et al., 2013] (all estimate ~1 TN/m, which equates to 5 MPa over a 200 km thick lithosphere). Furthermore, higher deviatoric stress would require higher strain rates—precluded by geodesy—or bulk viscosities beyond the $10^{22}\text{--}10^{24}$ Pas inferred by other means [Walcott, 1970; Forte et al., 2007; Boyd et al., 2015]. Lastly, the background $\sigma_{H\max}$ trend (N64E) suggested by CEUS moment tensors (Figure 1) matches that predicted by tectonic and convective models [Forte et al., 2007; Humphreys and Coblenz, 2007].

4.3. Gravity-Derived Stress

Lateral variations in lithostatic pressure produce horizontal stress, and departures from local isostasy must be offset by flexural stress. We estimate the gravity-derived stress tensor (Figure 3a) using a PyLith finite element model [Aagaard et al., 2013], dividing the study area into $10 \times 10 \times 10$ km hexahedral cells and extending it 200 km in each direction to mitigate edge effects. The model initializes with isotropic stress equal to average

lithostatic pressure at any given depth; deviations from this average density structure produce deviatoric loads [McGarr, 1988].

Dirichlet boundary conditions are applied at the sides and bottom. The upper surface is traction free. The upper 20 km is elastic, with Maxwell viscoelastic material below (viscosity = 10^{23} Pa s, as justified above). Since we seek a quasi-static solution for the loading stress, however, rheology is of negligible importance, and this viscosity independence is greater still over the 1 order of magnitude range that we estimate above. And as shown by Grana and Richardson [1996], this loading may persist for >100 m.y.

Our modeling predicts that gravity-derived loading (Figure 3a) is similar in magnitude (1 MPa) to plate-boundary loading and basal shear. Yet although gravity-derived stress is elevated at the NMSZ, we also find that this tensor alone does not reproduce $\sigma_{H\max}$ observations from moment tensors.

5. Stress Model for the NMSZ and Surroundings

The net stress tensor is the sum of those due to density variations and far-field stress. The latter is assumed to be N64E compression, the optimal $\sigma_{H\max}$ trend in the CEUS. Because the magnitudes of the deviatoric components of the two are similar, the net deviatoric stress is greatest where they interfere constructively. (Here we use a far-field stress of 3.0 MPa, a value appropriate for either plate-boundary loading or basal shear. We conduct tests (see supporting information) with far-field stress ranging from 0.1 to 10 MPa, and 3 MPa maximizes the fit between observed and predicted principal stress directions, although results are similar for 2 to 5 MPa.)

Throughout much of the Mississippi Embayment, low-elevation and low-density sediments create rift-normal gravity-derived compression (Figure 3a). At the NMSZ, however, the anomalously dense lower crust not only elevates gravity-derived $\sigma_{H\max}$ (Figure 3a) but also rotates it to be more constructive with regional stress. Net (predicted) σ_1 is roughly E-W, and at 6 MPa is the greatest deviatoric stress (i.e., fastest fault reloading) in the region (Figure 4).

Moreover, predicted and independently observed $\sigma_{H\max}$ directions closely agree across the region (Figure 4). Specifically, our model predicts (1) NE-SW $\sigma_{H\max}$ in eastern Missouri, (2) ENE-WSW $\sigma_{H\max}$ in the Wabash Valley seismic zone, and (3) the counterclockwise rotation of $\sigma_{H\max}$ from ENE to NE in western Alabama.

The fact that our model predicts not only maximal deviatoric stresses that coincide with the most concentrated seismicity but also variations in $\sigma_{H\max}$ that roughly agree with observations across the region suggests that there is no need for anomalously weak faults or lithosphere, favorable small-scale convection, or transient perturbations to explain the location and style of NMSZ seismicity. Nevertheless, erosion due to deglaciation—both melt pulses and drainage reorganization—would increase deviatoric stress in the NMSZ and increase Coulomb stress on faults. Holocene removal of 30 m of sediment [Van Arsdale et al., 2014] decreased vertical stress by 0.6 MPa (increasing deviatoric stress by 10%) and potentially triggered the late Quaternary increase in NMSZ activity [Calais et al., 2010].

In addition to the NMSZ, our model predicts elevated stress along the multiply reactivated [Cox et al., 2013; Hao et al., 2015] Alabama-Oklahoma Transform (Figure 1d). The Guy-Greenbrier, Arkansas, earthquake swarms coincide with another locus of elevated stress (Figure 3d), suggesting that body forces influence both natural and induced seismicities.

By contrast, despite liquefaction evidence of strong Holocene shaking [e.g., Obermeier et al., 1993; Munson et al., 1997] the Wabash Valley seismic zone may not be subject to anomalously high long-term stress. Seismicity there may instead reflect optimally oriented faults in the regional stress field, transient perturbations due to glacial isostatic adjustment [Grollimund and Zoback, 2001] or deglacial erosion [e.g., Calais et al., 2010], or an active phase of naturally periodic intraplate seismicity [Kenner and Segall, 2000; Clark et al., 2012].

6. Modeled Stress and Geodetic/Geologic Strain Rates

The large earthquakes in the NMSZ have puzzled geodesists in recent decades because the rate of strain accumulation is low ($\sim 10^{-9}/\text{yr}$) if even detectable [Newman et al., 1999; Calais et al., 2006; Frankel et al.,

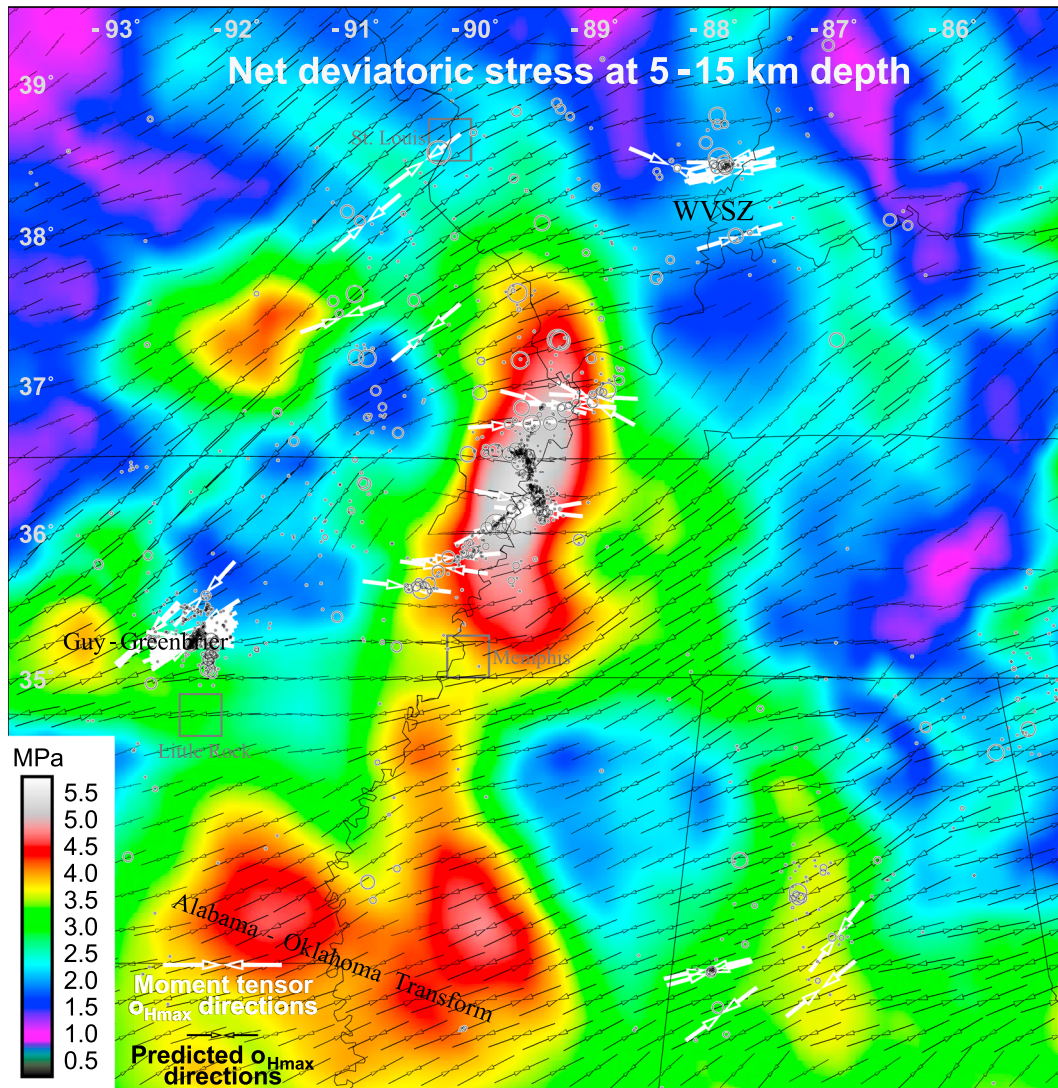


Figure 4. Net deviatoric stress, the sum of gravity-derived and tectonic stresses (Figures 3a and 3c, shown with 3 MPa of far-field stress; the mean of the six acceptable models shown in Figure 3c). Modeled principal stress directions (black) closely agree with independent moment tensor observations (white). The NMSZ hosts a regionally maximal deviatoric stress, which is well oriented to exploit existing faults.

2012; *Craig and Calais, 2014; Boyd et al., 2015*], issues of postseismic deformation notwithstanding. Additionally, the vertical throw on individual faults imaged in seismic data is generally ~100 m or less [Schweig and Ellis, 1994; Van Arsdale, 2000; Odum et al., 2010; Hao et al., 2013, 2015]. Yet we argue that deviatoric stress in the NMSZ is elevated and, implicitly, that the source of this stress is likely Middle/Late Cretaceous in age. As such, geodetic and geologic strain rates should also be elevated. But what strain rates does our model predict? And how much fault offset is expected since the Middle/Late Cretaceous?

In grossly Newtonian media (equation (3)) with viscosity 3×10^{23} Pa s (our inferred upper bound), 6 MPa of deviatoric stress causes 6×10^{-10} strain/yr, a rate certainly permitted by geodetic data. Integration over 100 m.y. predicts 6% strain or some 6 km of ~E-W shortening across the ~100 km wide Mississippi Embayment. Although the vertical throw imaged on faults is small, oblique motion is more cryptic. *Pratt et al. [2012]* argue that much of the deformation along the CWG occurs on positive flower structures and that ~10–12.5 km of total dextral displacement has accrued, likely partitioned across some half-dozen subparallel faults [*Pratt, 1994; Johnston and Schweig, 1996; Cox et al., 2006*]. Unconformities in Joiner ridge and the Manila high [*Odum et al., 2010*] and topography in the Eocene pop-up Crowley's Ridge [*Csontos et al., 2008*]

are offset by ~10 and 5 km, respectively. Given the N55E strike of the CWG, these offsets alone record 8–10 km, 8 km, and 4 km of east-west shortening. The 6% strain that we estimate for the past 100 m.y. is similar, if not less.

Thus, Holocene slip rates in the NMSZ likely reflect naturally periodic intraplate seismicity [Kenner and Segall, 2000; Clark et al., 2012] and exceed long-term rates [Schweig and Ellis, 1994]. Nevertheless, our models predict that these long-term rates themselves are greater than anywhere in the surrounding region, scaling roughly linearly with the long-term deviatoric stress (e.g., some 6 times the long-term rate in the stable regions of central Missouri, where net loading is ~1 MPa).

7. Conclusions

The density of the CEUS crust and upper mantle causes variations in both the direction and magnitude of deviatoric stress in the seismogenic crust. At the NMSZ in particular, low-density sedimentary rocks and anomalously dense lower crust create ~5 MPa of horizontal compression that interferes constructively with far-field stress. As a result, the NMSZ is subject to the highest deviatoric stress in the region, and this stress is (re)oriented favorably to exploit faults inherited from prior tectonism. Secular perturbations may push NMSZ faults closer to or farther from failure, but lithospheric structure causes a long-term and dominant elevation of fault loading and therefore seismicity rates.

Acknowledgments

The mean density model and the modeled stress tensors are included in the supporting information. W.L. was funded by the Mendenhall Postdoctoral Fellowship. The authors thank Morgan Page and Art McGarr for presubmission reviews.

References

- Aagaard, B. T., M. G. Knepley, and C. A. Williams (2013), A domain decomposition approach to implementing fault slip in finite-element models of quasi-static and dynamic crustal deformation, *J. Geophys. Res. Solid Earth*, 118, 3059–3079, doi:10.1002/jgrb.50217.
- Becker, T. W., and R. J. O'Connell (2001), Predicting plate velocities with mantle circulation models, *Geochem. Geophys. Geosyst.*, 2(12), 1060, doi:10.1029/2001GC000171.
- Boyd, O. S., and C. H. Cramer (2014), Estimating earthquake magnitudes from reported intensities in the Central and Eastern United States, *Bull. Seismol. Soc. Am.*, 104(4), 1709–1722, doi:10.1785/0120120352.
- Boyd, O. S., R. Smalley Jr., and Y. Zeng (2015), Crustal deformation in the New Madrid seismic zone and the role of postseismic processes, *J. Geophys. Res. Solid Earth*, 120, 5782–5803, doi:10.1002/2015JB012049.
- Brocher, T. M. (2005), Empirical relations between elastic wavespeeds and density in the Earth's crust, *Bull. Seismol. Soc. Am.*, 95(6), 2081–2092, doi:10.1785/01200500077.
- Calais, E., J. Y. Han, C. DeMets, and J. M. Nocquet (2006), Deformation of the North American plate interior from a decade of continuous GPS measurements, *J. Geophys. Res.*, 111, B06402, doi:10.1029/2005JB004253.
- Calais, E., A. M. Freed, R. Van Arsdale, and S. Stein (2010), Triggering of New Madrid seismicity by late-Pleistocene erosion, *Nature*, 466(7306), 608–611, doi:10.1038/nature09258.
- Christensen, N. I. (1996), Poisson's ratio and crustal seismology, *J. Geophys. Res.*, 101(B2), 3139–3156, doi:10.1029/95JB03446.
- Clark, D., A. McPherson, and R. Van Dissen (2012), Long-term behaviour of Australian stable continental region (SCR) faults, *Tectonophysics*, 566–567, 1–30.
- Cox, R. T., and R. Van Arsdale (2002), The Mississippi Embayment, North America: A first order continental structure generated by the Cretaceous superplume mantle event, *J. Geodyn.*, 34, 163–176.
- Cox, R. T., J. Cherryhomes, J. B. Harris, D. Larsen, R. B. Van Arsdale, and S. L. Forman (2006), Paleoseismology of the southeastern Reelfoot Rift in western Tennessee and implications for intraplate fault zone evolution, *Tectonics*, 25, TC3019, doi:10.1029/2005TC001829.
- Cox, R. T., J. L. Hall, and C. S. Gardner (2013), Tectonic history and setting of a seismogenic intraplate fault system that lacks microseismicity: The Saline River fault system, southern United States, *Tectonophysics*, 608(C), 252–266, doi:10.1016/j.tecto.2013.09.031.
- Craig, T. J., and E. Calais (2014), Strain accumulation in the New Madrid and Wabash Valley seismic zones from 14 years of continuous GPS observation, *J. Geophys. Res. Solid Earth*, 119, 9110–9129, doi:10.1002/2014JB011498.
- Cramer, C. H., and O. S. Boyd (2014), Why the New Madrid earthquakes are M 7–8 and the Charleston earthquake is M 7, *Bull. Seismol. Soc. Am.*, 104(6), 2884–2903, doi:10.1785/0120120257.
- Csontos, R., R. Van Arsdale, R. Cox, and B. Waldron (2008), Reelfoot rift and its impact on Quaternary deformation in the central Mississippi River valley, *Geosphere*, 4(1), 145–158, doi:10.1130/GES00107.1.
- Dater, D., D. Metzger, and A. Hittelman (1999), *Dater: Land and Marine Gravity* [CD-ROM], Natl. Geophys. Data Cent., Boulder, Colo.
- England, R. W., G. Houseman, and L. J. Sonder (1985), Length scales for continental deformation in convergent, divergent, and strike-slip environments: Analytical and approximate solutions for a thin viscous sheet model, *J. Geophys. Res.*, 90, 3551–3557, doi:10.1029/JB090iB05p03551.
- Ervin, C. P., and L. D. McGinnis (1975), Reelfoot rift: Reactivated precursor to the Mississippi embayment, *Geol. Soc. Am. Bull.*, 86(9), 1287–1295, doi:10.1130/0016-7606.
- Flesch, L. M., W. E. Holt, A. J. Haines, L. Wen, and B. Shen-Tu (2007), The dynamics of western North America: Stress magnitudes and the relative role of gravitational potential energy, plate interaction at the boundary and basal tractions, *Geophys. J. Int.*, 169(3), 866–896, doi:10.1111/j.1365-246X.2007.03274.x.
- Forte, A. M., J. X. Mitrovica, R. Moucha, N. A. Simmons, and S. P. Grand (2007), Descent of the ancient Farallon slab drives localized mantle flow below the New Madrid seismic zone, *Geophys. Res. Lett.*, 34, L04308, doi:10.1029/2006GL027895.
- Frankel, A., R. Smalley, and J. Paul (2012), Significant motions between GPS sites in the New Madrid Region: Implications for seismic hazard, *Bull. Seismol. Soc. Am.*, 102(2), 479–489, doi:10.1785/0120100219.
- Ghosh, A., W. E. Holt, and L. Wen (2013), Predicting the lithospheric stress field and plate motions by joint modeling of lithosphere and mantle dynamics, *J. Geophys. Res. Solid Earth*, 118, 346–368, doi:10.1029/2012JB009516.

- Ginzburg, A., W. D. Mooney, A. W. Walter, W. J. Lutter, and J. H. Healy (1983), Deep structure of northern Mississippi Embayment, *AAPG Bull.*, 67(11), 2031–2046, doi:10.1306/ad4608be-16f7-11d7-8645000102c1865d.
- Grana, J. P., and R. M. Richardson (1996), Tectonic stress within the New Madrid seismic zone, *J. Geophys. Res.*, 101, 5445–5458, doi:10.1029/95JB03255.
- Grollimund, B., and M. D. Zoback (2001), Did deglaciation trigger intraplate seismicity in the New Madrid seismic zone?, *Geology*, 29(2), 175–178, doi:10.1130/0091-7613(2001)029<0175:DDTISI>2.0.CO;2.
- Hao, Y., M. B. Magnani, K. McIntosh, B. Waldron, and L. Guo (2013), Quaternary deformation along the Meeman-Shelby Fault near Memphis, Tennessee, imaged by high-resolution marine and land seismic reflection profiles, *Tectonics*, 32, 501–515, doi:10.1002/tect.20042.
- Hao, Y., K. McIntosh, and M. B. Magnani (2015), Long-lived deformation in the southern Mississippi embayment revealed by high-resolution seismic reflection and sub-bottom profiler data, *Tectonics*, 34, 555–570, doi:10.1002/2014TC003750.
- Hatcher, R. D., W. A. Thomas, and G. W. Viele (1989), *The Appalachian-Ouachita Orogen in the United States*, *Geol. of North Am.*, Geol. Soc. of Am, Boulder, Colo.
- Hermann, R. B. (2015), Moment tensors for North America. [Available at http://www.eas.slu.edu/eqc/eqc_mt/MECH.NA/MECHFIG/mech.html, Last accessed 1/20/2015.]
- Hough, S. E., and M. Page (2011), Toward a consistent model for strain accrual and release for the New Madrid seismic zone, Central United States, *J. Geophys. Res.*, 116, B03311, doi:10.1029/2010JB007783.
- Humphreys, E. D., and D. D. Coblenz (2007), North American dynamics and western U.S. tectonics, *Rev. Geophys.*, 45, RG3001, doi:10.1029/2005RG000181.
- Hurd, O., and M. D. Zoback (2012a), Regional stress orientations and slip compatibility of earthquake focal planes in the New Madrid seismic zone, *Seismol. Res. Lett.*, 83(4), 672–679, doi:10.1785/0220110122.
- Hurd, O., and M. D. Zoback (2012b), Intraplate earthquakes, regional stress and fault mechanics in the Central and Eastern U.S. and southeastern Canada, *Tectonophysics*, 581(C), 182–192, doi:10.1016/j.tecto.2012.04.002.
- Johnson, G. A., S. P. Horton, M. Withers, and R. Cox (2014), Earthquake focal mechanisms in the New Madrid seismic zone, *Seismol. Res. Lett.*, 85(2), 257–267, doi:10.1785/0220130140.
- Johnston, A. C. (1996), Seismic moment assessment of earthquakes in stable continental regions—III. New Madrid 1811–1812, Charleston 1886 and Lisbon 1755, *Geophys. J. Int.*, 126(2), 314–344, doi:10.1111/j.1365-246X.1996.tb05294.x.
- Johnston, A. C., and E. S. Schweig (1996), The enigma of the New Madrid earthquakes of 1811–1812, *Annu. Rev. Earth Planet. Sci.*, 24, 339–384, doi:10.1146/annurev.earth.24.1.339.
- Jones, C. H., J. R. Unruh, and L. J. Sonder (1996), The role of gravitational potential energy in active deformation in the southwestern United States, *Nature*, 381, 1–5.
- Kenner, S. J., and A. P. Segall (2000), A mechanical model for intraplate earthquakes: Application to the New Madrid seismic zone, *Science*, 289(5488), 2329–2332, doi:10.1126/science.289.5488.2329.
- Kirby, J. F., and C. J. Swain (2009), A reassessment of spectral T_e estimation in continental interiors: The case of North America, *J. Geophys. Res.*, 114, B08401, doi:10.1029/2009JB006356.
- Langenheim, V. E., and T. G. Hildenbrand (1997), Commerce geophysical lineament—Its source, geometry, and relation to the Reelfoot rift and New Madrid seismic zone, *Geol. Soc. Am. Bull.*, 109(5), 580–595, doi:10.1130/0016-7606(1997)109<0580:CGLISG>2.3.CO;2.
- Lee, C.-T. A. (2003), Compositional variation of density and seismic velocities in natural peridotites at STP conditions: Implications for seismic imaging of compositional heterogeneities in the upper mantle, *J. Geophys. Res.*, 108(B9), 2441, doi:10.1029/2003JB002413.
- Levandowski, W., O. Boyd, R. Briggs, and R. Gold (2015), A random-walk algorithm for modeling lithospheric density and the role of body forces in the evolution of the Midcontinent Rift, *Geochem. Geophys. Geosyst.*, 16, 4084–4107, doi:10.1002/2015GC005961.
- Liu, L., and M. D. Zoback (1997), Lithospheric strength and intraplate seismicity in the New Madrid seismic zone, *Tectonics*, 16, 585–595, doi:10.1029/97TC01467.
- Luttrell, K., and D. Sandwell (2012), Constraints on 3-D stress in the crust from support of mid-ocean ridge topography, *J. Geophys. Res.*, 117, B04402, doi:10.1029/2011JB008765.
- McGarr, A. (1988), On the state of lithospheric stress in the absence of applied tectonic forces, *J. Geophys. Res.*, 93, 13,609–13,617, doi:10.1029/JB093iB11p13609.
- Mooney, W. D., M. C. Andrews, A. Ginzburg, D. A. Peters, and R. M. Hamilton (1983), Crustal structure of the northern Mississippi Embayment and a comparison with other continental rift zones, *Tectonophysics*, 94(1–4), 327–348, doi:10.1016/0040-1951(83)90023-9.
- Munson, P. J., S. F. Obermeier, C. A. Munson, and E. R. Hajic (1997), Liquefaction evidence for Holocene and latest Pleistocene seismicity in the Southern Halves of Indiana and Illinois: A preliminary overview, *Seismol. Res. Lett.*, 68(4), 521–536.
- Newman, A., S. Stein, J. Weber, J. Engeln, A. Mao, and T. Dixon (1999), Slow deformation and lower seismic hazard at the New Madrid seismic zone, *Science*, 284(5414), 619–621, doi:10.1126/science.284.5414.619.
- Obermeier, S. F., J. R. Martin, A. D. Frankel, T. L. Youd, P. J. Munson, C. A. Munson, and E. C. Pond (1993), Liquefaction evidence for one or more strong Holocene earthquakes in the Wabash Valley of southern Indiana and Illinois, with a preliminary estimate of magnitude, *U.S. Geol. Surv. Prof. Pap.*, 1536, 27.
- Odum, J. K., W. J. Stephenson, and R. A. Williams (2010), Multisource, high-resolution seismic-reflection imaging of Meeman-Shelby fault and a possible tectonic model for a Joiner Ridge-Manila high stepover structure in the upper Mississippi Embayment region, *Seismol. Res. Lett.*, 81(4), 647–663, doi:10.1785/gssrl.81.4.647.
- Petersen, M. D., et al. (2014), Documentation for the 2014 update of the United States national seismic hazard maps, *USGS Open File Rep. 2014-1091*, doi:10.3133/ofr20141091.
- Pollitz, F. F., and W. D. Mooney (2014), Seismic structure of the Central US crust and shallow upper mantle: Uniqueness of the Reelfoot Rift, *Earth Planet. Sci. Lett.*, 402, 157–166, doi:10.1016/j.epsl.2013.05.042.
- Pollitz, F. F., and W. D. Mooney (2016), Seismic velocity structure of the crust and shallow mantle of the Central and Eastern United States by seismic surface-wave imaging, *Geophys. Res. Lett.*, 43, 118–126, doi:10.1002/2015GL066637.
- Pollitz, F. F., L. Kellogg, and R. Bürgmann (2001), Sinking mafic body in a reactivated lower crust: A mechanism for stress concentration at the New Madrid seismic zone, *Bull. Seismol. Soc. Am.*, 91(6), 1882–1897, doi:10.1785/0120000277.
- Pratt, T. L. (1994), How old is the New Madrid seismic zone?, *Seismol. Res. Lett.*, 65(2), 172–179, doi:10.1785/gssrl.65.2.172.
- Pratt, T. L., R. A. Williams, J. K. Odum, and W. J. Stephenson (2012), Origin of the Blytheville Arch, and long-term displacement on the New Madrid seismic zone, central United States, *Geol. Soc. Am. Spec. Pap.*, 493, 1–15, doi:10.1130/2012.2493(01).
- Ramirez-Guzmán, L., O. S. Boyd, S. Hartzell, and R. A. Williams (2012), Seismic velocity model of the Central United States (version 1): Description and simulation of the 18 April 2008 Mt. Carmel, Illinois, earthquake, *Bull. Seismol. Soc. Am.*, 102(6), 2622–2645, doi:10.1785/0120110303.

- Richardson, R. M. (1992), Ridge forces, absolute plate motions, and the intraplate stress field, *J. Geophys. Res.*, 97, 11,739–11,748, doi:10.1029/91JB00475.
- Schmandt, B., and F.-C. Lin (2014), *P* and *S* wave tomography of the mantle beneath the United States, *Geophys. Res. Lett.*, 41, 6342–6349, doi:10.1002/2014GL061231.
- Schutt, D. L., and C. E. Lesser (2010), Compositional trends among Kaapvaal Craton garnet peridotite xenoliths and their effects on seismic velocity and density, *Earth Planet. Sci. Lett.*, 300(3-4), 367–373, doi:10.1016/j.epsl.2010.10.018.
- Schweig, E. S., and M. A. Ellis (1994), Reconciling short recurrence intervals with minor deformation in the New Madrid seismic zone, *Science*, 264(5163), 1308–1311, doi:10.1126/science.264.5163.1308.
- Shumway, A. M. (2008), Focal mechanisms in the Northeast New Madrid seismic zone, *Seismol. Res. Lett.*, 79(3), 469–477, doi:10.1785/gssrl.79.3.469.
- Turcotte, D. L., and G. Schubert (2002), *Geodynamics*, 2nd ed., Cambridge Univ. Press, Cambridge.
- Tuttle, M. P., E. S. Schweig, J. D. Sims, R. H. Lafferty, L. W. Wolf, and M. L. Haynes (2002), The earthquake potential of the New Madrid seismic zone, *Bull. Seismol. Soc. Am.*, 92(6), 2080–2089, doi:10.1785/0120010227.
- Tuttle, M. P., E. S. Schweig III, J. Campbell, P. M. Thomas, J. D. Sims, and R. H. Lafferty III (2005), Evidence for New Madrid earthquakes in A.D. 300 and 2350 B.C., *Seismol. Res. Lett.*, 76(4), 489–501, doi:10.1785/gssrl.76.4.489.
- Van Arsdale, R. (2000), Displacement history and slip rate on the Reelfoot fault of the New Madrid seismic zone, *Eng. Geol.*, 55, 219–226, doi:10.1016/S0013-7952(99)00093-9.
- Van Arsdale, R. B., W. B. Cupples, and R. M. Csontos (2014), Pleistocene–Holocene transition in the central Mississippi River valley, *Geomorphology*, 214, 270–282, doi:10.1016/j.geomorph.2014.02.011.
- Vavryčuk, V. (2014), Iterative joint inversion for stress and fault orientations from focal mechanisms, *Geophys. J. Int.*, 199(1), 69–77, doi:10.1093/gji/ggu224.
- Walcott, R. I. (1970), Flexural rigidity, thickness, and viscosity of the lithosphere, *J. Geophys. Res.*, 75, 3941–3954, doi:10.1029/JB075i020p03941.
- Watts, A. B. (2001), *Isostasy and Flexure of the Lithosphere*, 458 pp., Cambridge Univ. Press, Cambridge.
- Watts, A. B. (2012), Global elastic thickness point data and grid. [Available at earth.ox.ac.uk/~tony/watts/downloads.htm, Last accessed 11/22/12.]
- Zoback, M. L., and J. Townend (2001), Implications of hydrostatic pore pressures and high crustal strength for the deformation of intraplate lithosphere, *Tectonophysics*, 336(1–4), 19–30, doi:10.1016/S0040-1951(01)00091-9.
- Zoback, M. L., and M. D. Zoback (1980), State of stress in the conterminous United States, *J. Geophys. Res.*, 85, 6113–6156, doi:10.1029/JB085iB11p06113.